

3D Dynamic Point Cloud Denoising via Spatial-Temporal Graph Learning

Wei Hu, *Member, IEEE*, Qianjiang Hu, *Student Member, IEEE*, Zehua Wang, *Student Member, IEEE*,
and Xiang Gao, *Student Member, IEEE*

Abstract—The prevalence of accessible depth sensing and 3D laser scanning techniques has enabled the convenient acquisition of 3D dynamic point clouds, which provide efficient representation of arbitrarily-shaped objects in motion. Nevertheless, dynamic point clouds are often perturbed by noise due to hardware, software or other causes. While a plethora of methods have been proposed for static point cloud denoising, few efforts are made for the denoising of dynamic point clouds with varying number of irregularly-sampled points in each frame. In this paper, we represent dynamic point clouds naturally on graphs and address the denoising problem by inferring the underlying graph via spatio-temporal graph learning, exploiting both the intra-frame similarity and inter-frame consistency. Firstly, assuming the availability of a relevant feature vector per node, we pose spatial-temporal graph learning as optimizing a Mahalanobis distance metric M , which is formulated as the minimization of graph Laplacian regularizer. Secondly, to ease the optimization of the symmetric and positive definite metric matrix M , we decompose it into $M = R^T R$ and solve R instead via proximal gradient. Finally, based on the spatial-temporal graph learning, we formulate dynamic point cloud denoising as the joint optimization of the desired point cloud and underlying spatio-temporal graph, which leverages both intra-frame affinities and inter-frame consistency and is solved via alternating minimization. Experimental results show that the proposed method significantly outperforms independent denoising of each frame from state-of-the-art static point cloud denoising approaches.

Index Terms—Dynamic point cloud denoising, spatial-temporal graph learning, Mahalanobis distance metric decomposition, graph Laplacian regularizer

I. INTRODUCTION

The maturity of depth sensing and 3D laser scanning techniques has enabled convenient acquisition of 3D dynamic point clouds, a natural representation for arbitrarily-shaped objects varying over time [1]. A dynamic point cloud consists of a sequence of static point clouds, each of which is composed of a set of points defined on irregular grids, as shown in Fig. 1. Each point has geometry information (*i.e.*, 3D coordinates) and possibly attribute information such as color. Because of the efficient representation, dynamic point clouds have been widely applied in various fields, such as 3D immersive telepresence, navigation for autonomous vehicles, gaming and animation [2].

Point clouds are often perturbed by noise, which comes from hardware, software or other causes. Hardware wise, noise occurs due to the inherent limitations of the acquisition equipment, as demonstrated in Fig. 1. Software wise, in the case of generating point clouds with existing algorithms, points may locate somewhere completely wrong due to imprecise triangulation (*e.g.*, a false epipolar matching). Due to the



Fig. 1: Three frames (0000, 0010, 0020) in the dynamic point cloud sequence *Phil* [3], which is captured by four frontal RGBD cameras. The hands are noisy in particular.

irregular sampling and varying number of points in each frame, dynamic point cloud denoising is quite challenging to address.

However, few efforts are made for the denoising of *dynamic* point clouds in the literature, while many approaches have been proposed for static point cloud denoising. Existing denoising methods for static point clouds mainly include moving least squares (MLS)-based methods [4]–[6], locally optimal projection (LOP)-based methods [7]–[9], sparsity-based methods [10], [11], non-local similarity-based methods [12], [13], and graph-based methods [14]–[17]. Whereas it is possible to apply existing static point cloud denoising methods to each frame of a dynamic point cloud sequence independently, the *inter-frame correlation* would be neglected, which may lead to inconsistent denoising results in the temporal domain.

To this end, we propose to exploit inter-frame correlation for dynamic point cloud denoising, which *not only enforces the temporal consistency but also provides additional temporal information for denoising*. Since point clouds are irregular, we represent dynamic point clouds naturally on *spatio-temporal graphs*, where each node represents a point and each edge captures the similarity between a pair of spatially or temporally adjacent points. In this paper, we focus on the geometry of point clouds, and thus the corresponding graph signal refers to the 3D Cartesian coordinates of points. Further, assuming a feature vector per node is available, we propose to infer the underlying graph representation via *spatial-temporal graph learning*, which is posed as the optimization of a Mahalanobis distance metric [18]. We then reconstruct dynamic point clouds by regularization from the learned graph representation, exploring both the intra-frame affinities and inter-frame correlation.

Specifically, we first propose spatial-temporal graph learning assuming the availability of relevant features $\mathbf{f}_i \in \mathbb{R}^K$ per node i . Since an edge weight characterizes pairwise similar-

ities between nodes, it is common to define an edge weight as a function of the feature distance. Given two connected nodes i and j and their feature difference $\mathbf{f}_i - \mathbf{f}_j$, we assume the edge weight $w_{i,j} = \exp\{-(\mathbf{f}_i - \mathbf{f}_j)^\top \mathbf{M}(\mathbf{f}_i - \mathbf{f}_j)\}$, where $\mathbf{M} \in \mathbb{R}^{K \times K}$ is the *Mahalanobis distance* metric matrix [18]. Considering a target point cloud signal with N points $\mathbf{z} \in \mathbb{R}^N$, we seek to optimize \mathbf{M} by minimizing the *Graph Laplacian Regularizer* (GLR) [19] $\mathbf{z}^\top \mathbf{L}(\mathbf{M})\mathbf{z}$, which measures the smoothness of the signal \mathbf{z} with respect to the graph Laplacian matrix \mathbf{L} [20]. Further, since \mathbf{M} is symmetric and positive definite, we decompose it as $\mathbf{M} = \mathbf{R}^\top \mathbf{R}$, $\mathbf{R} \in \mathbb{R}^{K \times K}$, so as to remove the constraint of positive definiteness for computation efficiency. Hence, given each target frame and its previous reconstructed frame in the input dynamic point cloud, we cast spatial-temporal graph learning as the estimation of the distance metrics $\{\mathbf{R}_s, \mathbf{R}_t\}$ from spatially and temporally neighboring points respectively, with $\mathbf{R}_s \in \mathbb{R}^{K \times K}$ as the spatial distance metric and $\mathbf{R}_t \in \mathbb{R}^{K \times K}$ as the temporal distance metric. We then propose an algorithm to optimize the distance metrics via proximal gradient descent [21].

Secondly, based on the spatial-temporal graph learning, we formulate dynamic point cloud denoising as the joint optimization of the desired point cloud and underlying spatial-temporal graph representation. To exploit the intra-frame correlation, we first divide each frame into overlapping patches. Each irregular patch is defined as a local point set consisting of a centering point and its k -nearest neighbors. For each target patch in the current noisy frame, we search for its most similar patches to exploit the intra-frame correlation, and search for its corresponding patch in the previously reconstructed frame to explore the inter-frame correlation. Given the searched patches, we construct spatio-temporal edge connectivities based on patch similarity. Then we regularize the formulation by smoothness of similar patches in the current frame via GLR as well as temporal consistency over corresponding patches with respect to the underlying spatio-temporal graph.

Finally, we propose an efficient algorithm to address the above problem formulation. We design an alternating minimization algorithm to optimize the underlying frame and spatial-temporal graph alternately. When the underlying frame is initialized or fixed, the graph is optimized from the proposed spatio-temporal graph learning. When the graph is fixed, we update the underlying frame via a closed-form solution. Then we update patch construction, similar patch search and edge connectivities from each update of the underlying frame. The process is iterated until convergence. Experimental results show that the proposed method outperforms independent denoising of each frame from state-of-the-art static point cloud denoising approaches on nine widely employed dynamic point cloud sequences.

In summary, the main contributions of our work include:

- We propose spatio-temporal graph learning to address dynamic point cloud denoising. The key idea is to exploit the inter-frame correlation of irregular point clouds for temporal consistency, which is inferred via spatial-temporal graph learning.

- We pose spatial-temporal graph learning as the optimization of both spatial and temporal Mahalanobis distance metrics by minimizing Graph Laplacian Regularizer, where we decompose the positive-definite Mahalanobis distance metrics for computation efficiency.
- Based on the spatial-temporal graph learning, we formulate dynamic point cloud denoising as joint optimization of the desired point cloud and underlying graph representation, and acquire the solution via alternating minimization.

The outline of this paper is as follows. We first review previous static point cloud denoising methods in Section II. Then we introduce basic concepts in spectral graph theory and GLR in Section III. Next, we elaborate on the proposed spatial-temporal graph learning in Section IV, and present the proposed dynamic point cloud denoising algorithm based on spatial-temporal graph learning in Section V. Finally, experimental results and conclusions are presented in Section VI and Section VII, respectively.

II. RELATED WORK

To the best of our knowledge, there are few efforts on dynamic point cloud denoising in the literature. [22] provides a short discussion on how the proposed graph-based static point cloud denoising naturally generalizes to time-varying inputs such as 3D dynamic point clouds. Therefore, we discuss previous works on *static* point cloud denoising, which can be divided into five classes: moving least squares (MLS)-based methods, locally optimal projection (LOP)-based methods, sparsity-based methods, non-local methods, and graph-based methods.

MLS-based methods. MLS-based methods aim to approximate a smooth surface from the input point cloud and minimize the geometric error of the approximation. Alexa *et al.* approximate with a polynomial function on a local reference domain to best fit neighboring points in terms of MLS [4]. Other similar solutions include algebraic point set surfaces (APSS) [5] and robust implicit MLS (RIMLS) [6]. However, this class of methods may lead to over-smoothing results.

LOP-based methods. LOP-based methods also employ surface approximation for denoising point clouds. Unlike MLS-based methods, the operator is non-parametric, which performs well in cases of ambiguous orientation. For instance, Lipman *et al.* define a set of points that represent the estimated surface by minimizing the sum of Euclidean distances to the data points [9]. The two branches of [9] are weighted LOP (WLOP) [8] and anisotropic WLOP (AWLOP) [7]. [8] produces a set of denoised, outlier-free and more evenly distributed particles over the original dense point cloud to keep the sample distance of neighboring points. [7] modifies WLOP with an anisotropic weighting function so as to preserve sharp features better. Nevertheless, LOP-based methods may also over-smooth point clouds.

Sparsity-based methods. These methods are based on sparse representation of point normals. Regularized by sparsity, a global minimization problem is solved to obtain sparse reconstruction of point normals. Then the positions of points

are updated by solving another global l_0 [23] or l_1 [10] minimization problem based on a local planar assumption. Mattei *et al.* [11] propose *Moving Robust Principal Components Analysis* (MRPCA) approach to denoise 3D point clouds via weighted l_1 minimization to preserve sharp features. However, when locally high noise-to-signal ratios yield redundant features, these methods may not perform well and lead to over-smoothing or over-sharpening [23].

Non-local methods. Inspired by non-local means (NLM) [24] and BM3D [25] image denoising algorithms, this class of methods exploit self-similarities among surface patches in a point cloud. Digne *et al.* utilize a NLM algorithm to denoise static point clouds [26], while Rosman *et al.* deploy a BM3D method [27]. Deschaud *et al.* extend non-local denoising (NLD) algorithm for point clouds, where the neighborhood of each point is described by the polynomial coefficients of the local MLS surface to compute point similarity [28]. [29] utilizes patch self-similarity and optimizes for a low rank (LR) dictionary representation of the extracted patches to smooth 3D patches. Nevertheless, the computational complexity of these methods is usually high.

Graph-based methods. This family of methods represent a point cloud on a graph, and design graph filters for denoising. Schoenberger *et al.* [22] construct a k -nearest-neighbor graph on the input point cloud and then formulate a convex optimization problem regularized by the gradient of the point cloud on the graph. Dinesh *et al.* [14] design a reweighted graph Laplacian regularizer for surface normals, which is deployed to formulate an optimization problem with a general lp-norm fidelity term that can explicitly model two types of independent noise. Zeng *et al.* [15] propose a low-dimensional manifold model (LDMM) with graph Laplacian regularization (GLR) and exploit self-similar surface patches for denoising. Instead of directly smoothing the 3D coordinates or surface normals, Duan *et al.* [16] estimate the local tangent plane of each point based on a graph, and then reconstruct 3D point coordinates by averaging their projections on multiple tangent planes. Hu *et al.* [17] propose feature graph learning to optimize edge weights given available signal(s) assumed to be smooth with respect to the graph. However, the temporal dependency is not exploited yet in this class of methods.

III. BACKGROUND ON SPECTRAL GRAPH THEORY

We represent dynamic point clouds on undirected graphs. An undirected graph $\mathcal{G} = \{\mathcal{V}, \mathcal{E}, \mathbf{A}\}$ is composed of a node set \mathcal{V} of cardinality $|\mathcal{V}| = n$, an edge set \mathcal{E} connecting nodes, and a weighted adjacency matrix \mathbf{A} . $\mathbf{A} \in \mathbb{R}^{n \times n}$ is a real and symmetric matrix, where $a_{i,j} \geq 0$ is the weight assigned to the edge (i, j) connecting nodes i and j . Edge weights often measure the similarity between connected nodes.

The graph Laplacian matrix is defined from the adjacency matrix. Among different variants of Laplacian matrices, the commonly used *combinatorial graph Laplacian* [30], [31] is defined as $\mathbf{L} := \mathbf{D} - \mathbf{A}$, where \mathbf{D} is the *degree matrix*—a diagonal matrix where $d_{i,i} = \sum_{j=1}^n a_{i,j}$.

Graph signal refers to data that resides on the nodes of a graph. In our case, the coordinates of each point in the input dynamic point cloud are the graph signal. A graph signal $\mathbf{z} \in$

\mathbb{R}^n defined on a graph \mathcal{G} is smooth with respect to the topology of \mathcal{G} if

$$\sum_{i \sim j} a_{i,j} (z_i - z_j)^2 < \epsilon, \quad (1)$$

where ϵ is a small positive scalar, and $i \sim j$ denotes two nodes i and j are one-hop neighbors in the graph. In order to satisfy (1), z_i and z_j have to be similar for a large edge weight $a_{i,j}$, and could be quite different for a small $a_{i,j}$. Hence, (1) enforces \mathbf{z} to adapt to the topology of \mathcal{G} , which is referred as *Graph Laplacian Regularizer* (GLR).

As $\mathbf{z}^T \mathbf{L} \mathbf{z} = \sum_{i \sim j} a_{i,j} (z_i - z_j)^2$ [32], (1) is concisely written as $\mathbf{z}^T \mathbf{L} \mathbf{z} < \epsilon$ in the sequel. This term will be employed as the objective of spatio-temporal graph learning and the prior in the problem formulation of dynamic point cloud denoising.

IV. SPATIAL-TEMPORAL GRAPH LEARNING

A. Formulation

Spatial-temporal graph learning involves the inference of both edge connectivities and edge weights. In this paper, we focus on *spatial-temporal edge weight learning* assuming the availability of connectivities in a spatial-temporal graph¹. Since an edge weight $a_{i,j}$ for nodes i and j describes the pairwise similarity between the two nodes, we essentially learn the *similarity distance metric*.

While there exist various distance metrics, such as the Euclidean distance and bilateral distance [33], we employ the *Mahalanobis distance* [18] widely used in the machine learning literature, which takes feature correlations into account. Assuming a feature vector $\mathbf{f}_i \in \mathbb{R}^K$ is associated with each node i , the Mahalanobis distance between nodes i and j is defined as

$$d_{\mathbf{M}}(\mathbf{f}_i, \mathbf{f}_j) = (\mathbf{f}_i - \mathbf{f}_j)^T \mathbf{M} (\mathbf{f}_i - \mathbf{f}_j), \quad (2)$$

where $\mathbf{M} \in \mathbb{R}^{K \times K}$ is the distance metric we aim to optimize. \mathbf{M} is required to be positive definite, *i.e.*, $\mathbf{M} \succ 0$.

Employing the commonly used Gaussian kernel [17], we formulate the edge weight as:

$$a_{i,j} = \exp \{-d_{\mathbf{M}}(\mathbf{f}_i, \mathbf{f}_j)\} \quad (3)$$

$$= \exp \{-(\mathbf{f}_i - \mathbf{f}_j)^T \mathbf{M} (\mathbf{f}_i - \mathbf{f}_j)\}. \quad (4)$$

We now pose an optimization problem for \mathbf{M} with GLR (1) as objective. we seek the optimal metric \mathbf{M} that yields the smallest GLR term given feature vector \mathbf{f}_i per node i and point cloud observation with n points $\{\mathbf{v}_i\}_{i=1}^n \in \mathbb{R}^{n \times 3}$, where $\mathbf{v}_i \in \mathbb{R}^3$ is the 3D coordinate vector of node i . Specifically, denote the inter-node sample difference square of observation \mathbf{z} in (1) by $d_{i,j} = \|\mathbf{v}_i - \mathbf{v}_j\|_2^2$, we have

$$\min_{\mathbf{M}} \sum_{i \sim j} \exp \{-(\mathbf{f}_i - \mathbf{f}_j)^T \mathbf{M} (\mathbf{f}_i - \mathbf{f}_j)\} d_{i,j} \quad (5)$$

$$\text{s.t. } \mathbf{M} \succ 0.$$

Minimizing (5) directly would lead to one pathological solution, *i.e.*, $m_{i,i} = \infty, \forall i$, resulting in edge weight $a_{i,j} = 0$. As discussed in [17], this means nodes in the graph are all

¹We propose efficient construction of edge connectivities in Section V.

isolated, defeating the goal of finding a similarity graph. To avoid this solution, we constrain the trace of \mathbf{M} to be smaller than a constant parameter $C > 0$, resulting in

$$\begin{aligned} \min_{\mathbf{M}} \sum_{i \sim j} \exp \{ -(\mathbf{f}_i - \mathbf{f}_j)^\top \mathbf{M} (\mathbf{f}_i - \mathbf{f}_j) \} d_{i,j} \\ \text{s.t. } \mathbf{M} \succ 0; \quad \text{tr}(\mathbf{M}) \leq C. \end{aligned} \quad (6)$$

It is nontrivial to solve \mathbf{M} in low complexity as \mathbf{M} is in the feasible space of a positive-definite cone. One naïve approach is to employ gradient descent and then map the solution to the feasible space by setting negative eigenvalues of \mathbf{M} to zero. Nevertheless, this would require eigen-decomposition of \mathbf{M} per iteration with complexity $\mathcal{O}(n^3)$. Instead, since \mathbf{M} is symmetric and positive definite, we propose to decompose \mathbf{M} into $\mathbf{M} = \mathbf{R}^\top \mathbf{R}$, where we consider $\mathbf{R} \in \mathbb{R}^{K \times K}$ assuming full rank². This leads to

$$\begin{aligned} d_{\mathbf{M}}(\mathbf{f}_i, \mathbf{f}_j) &= (\mathbf{f}_i - \mathbf{f}_j)^\top \mathbf{R}^\top \mathbf{R} (\mathbf{f}_i - \mathbf{f}_j) \\ &= (\mathbf{R}(\mathbf{f}_i - \mathbf{f}_j))^\top \mathbf{R} (\mathbf{f}_i - \mathbf{f}_j) \\ &= \|\mathbf{R}(\mathbf{f}_i - \mathbf{f}_j)\|_2^2, \end{aligned} \quad (7)$$

which can be viewed as a Euclidean distance of the linearly transformed feature distance via \mathbf{R} . The edge weight in (4) is then

$$a_{i,j} = \exp \{ -\|\mathbf{R}(\mathbf{f}_i - \mathbf{f}_j)\|_2^2 \}. \quad (8)$$

Substituting (7) into (6), we have

$$\begin{aligned} \min_{\mathbf{R}} \sum_{i \sim j} \exp \{ -\|\mathbf{R}(\mathbf{f}_i - \mathbf{f}_j)\|_2^2 \} d_{i,j} \\ \text{s.t. } \text{tr}(\mathbf{R}) \leq C; r_{i,i} \geq 0, \forall i. \end{aligned} \quad (9)$$

Here we further constrain each diagonal entry of \mathbf{R} to be non-negative. Otherwise, the diagonal entries might be negative with large absolute value that leads to infinite trace of \mathbf{M} . Now the feasible space is converted to a convex set of a polytope, which can be solved much more efficiently.

Further, we propose to learn *spatial* edge weights and *temporal* edge weights in spatio-temporal graph learning separately, which correspond to a spatial metric \mathbf{R}_s and a temporal metric \mathbf{R}_t respectively. Spatial edge weights are acquired by optimizing \mathbf{R}_s from node pairs $\{i, j\}$ within the same frame, while temporal edge weights are computed from \mathbf{R}_t optimized via temporally connected node pairs $\{i, j\}$. Given appropriate node pairs, the optimization algorithms of \mathbf{R}_s and \mathbf{R}_t are the same, which will be discussed next.

B. Optimization Algorithm

To solve the constrained optimization problem (9) efficiently, we employ a *proximal gradient* (PG) approach [21]. We first define an indicator function $I_S(\mathbf{R})$:

$$I_S(\mathbf{R}) = \begin{cases} 0, & \mathbf{R} \in \mathcal{S} \\ \infty, & \text{otherwise} \end{cases} \quad (10)$$

where

$$\mathcal{S} = \left\{ \mathbf{R} \mid \text{tr}(\mathbf{R}) \leq C; r_{i,i} \geq 0, \forall i \right\}. \quad (11)$$

We then rewrite (9) as an unconstrained problem by incorporating the indicator function $I_S(\mathbf{R})$ into the objective:

$$\min_{\mathbf{R}} \sum_{i \sim j} \exp \{ -\|\mathbf{R}(\mathbf{f}_i - \mathbf{f}_j)\|_2^2 \} d_{i,j} + I_S(\mathbf{R}). \quad (12)$$

The first term is convex with respect to \mathbf{R} and differentiable, while the second term $I_S(\mathbf{R})$ is convex but non-differentiable. we can thus employ PG to solve (12) as follows.

We first compute the gradient of the first term F with respect to \mathbf{R} :

$$\begin{aligned} \nabla F(\mathbf{R}) \\ = -2 \sum_{\{i,j\}} \mathbf{R}(\mathbf{f}_i - \mathbf{f}_j)(\mathbf{f}_i - \mathbf{f}_j)^\top \exp \{ -\|\mathbf{R}(\mathbf{f}_i - \mathbf{f}_j)\|_2^2 \} d_{i,j}. \end{aligned} \quad (13)$$

Next, we define a proximal mapping $\Pi_{I_S}(\mathbf{V})$ for the second term—indicator function $I_S(\mathbf{V})$ —which is a projection onto the linear set \mathcal{S} , *i.e.*,

$$\Pi_{I_S}(\mathbf{V}) = \begin{cases} \mathbf{V}, & \text{tr}(\mathbf{R}) \leq C, r_{i,i} \geq 0, \forall i \\ g(\mathbf{V}) - \alpha \cdot \text{diag}(g(\mathbf{V})), & \text{otherwise,} \end{cases} \quad (14)$$

where $g(\mathbf{V})$ is a function that projects all diagonal entries of \mathbf{V} to non-negative values, *i.e.*, $\max(r_{i,i}, 0), \forall i$. α is any positive root of $\text{tr}(g(\mathbf{V}) - \alpha \cdot \text{diag}(g(\mathbf{V}))) = C$.

Each iteration of the PG algorithm can be now written as:

$$\mathbf{R}^{l+1} = \Pi_{I_S}(\mathbf{R}^l - t \nabla F(\mathbf{R}^l)), \quad (15)$$

where t is the step size, and \mathbf{R}^l and \mathbf{R}^{l+1} are the solved metric at the l -th and $(l+1)$ -th iteration respectively. As discussed in [21], the algorithm will converge with rate $\mathcal{O}(1/l)$ for a fixed step size $t^l = t \in (0, 2/L]$, where L is a Lipschitz constant that requires computation of the Hessian of F . In our experiment, we choose a small step size t empirically, which is small enough to satisfy the Lipschitz smoothness of the objective function. In the first iteration, we initialize \mathbf{R} to be an identity matrix, and assign such a C that $\text{tr}(\mathbf{R}) \leq C$. We empirically find that the denoising results are relatively insensitive to C , as long as C is slightly larger than the dimension K of features per node.

V. PROPOSED DYNAMIC POINT CLOUD DENOISING

Leveraging on the proposed spatio-temporal graph learning, we propose a dynamic point cloud denoising algorithm to exploit the spatio-temporal correlation. A dynamic point cloud sequence $\mathcal{P} = \{\mathbf{U}_1, \mathbf{U}_2, \dots, \mathbf{U}_m\}$ consists of m frames of point clouds. The coordinates $\mathbf{U}_t = [\mathbf{u}_{t,1}, \mathbf{u}_{t,2}, \dots, \mathbf{u}_{t,n}]^\top \in \mathbb{R}^{n \times 3}$ denote the position of each point in the point cloud at frame t , in which $\mathbf{u}_{t,i} \in \mathbb{R}^3$ represents the coordinates of the i -th point in frame t . Let $\hat{\mathbf{U}}_t$ denote the ground truth coordinates of the t -th frame, and $\tilde{\mathbf{U}}_{t-1}$, $\tilde{\mathbf{U}}_t$ denote the noise-corrupted coordinates of the $(t-1)$ -th and t -th frame respectively. Given each noisy frame $\tilde{\mathbf{U}}_t$, we aim to recover its underlying signal \mathbf{U}_t , exploiting the intra-frame self-similarity in $\tilde{\mathbf{U}}_t$ as well as the inter-frame dependencies with the *reconstructed* previous frame $\tilde{\mathbf{U}}_{t-1}$.

²In general, \mathbf{R} can be a non-square matrix.

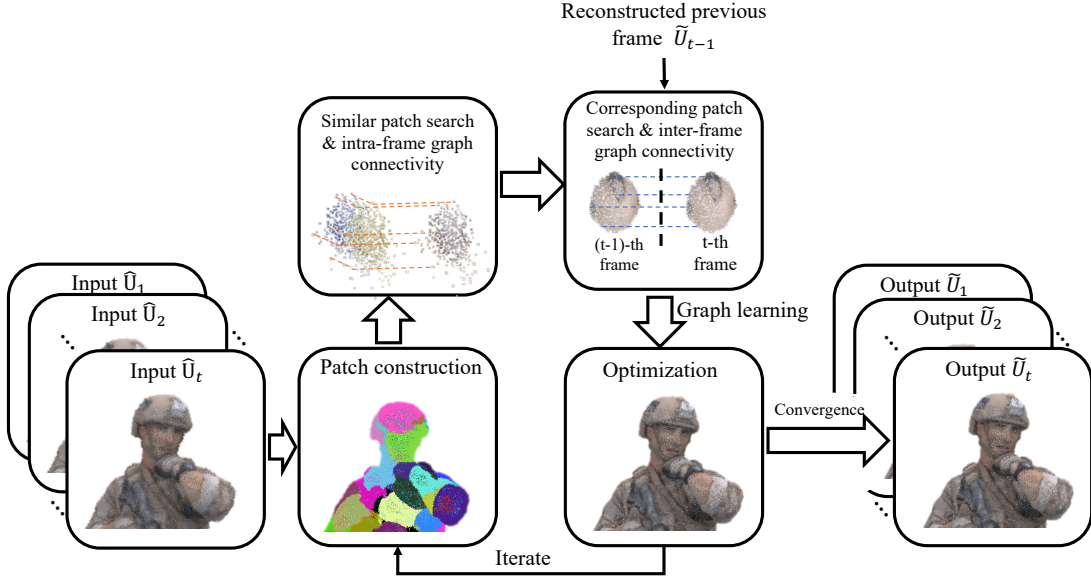


Fig. 2: The flowchart of the proposed dynamic point cloud denoising algorithm.

A. Patch Construction

In order to exploit local characteristics of point clouds, we model both intra-frame and inter-frame dependencies on *patch* basis. Unlike images or videos defined on regular grids, point clouds reside on irregular domain with uncertain local neighborhood, thus the definition of a patch is nontrivial. We define a patch $\mathbf{p}_{t,l} \in \mathbb{R}^{(k+1) \times 3}$ in point cloud $\hat{\mathbf{U}}_t$ as a local point set of $k+1$ points, consisting of a centering point $\mathbf{c}_{t,l} \in \mathbb{R}^3$ and its k -nearest neighbors in terms of Euclidean distance. Then the entire set of patches at frame t is

$$\mathbf{P}_t = \mathbf{S}_t \hat{\mathbf{U}}_t - \mathbf{C}_t, \quad (16)$$

where $\mathbf{S}_t \in \{0,1\}^{(k+1)M \times n}$ is a sampling matrix to select points from point cloud $\hat{\mathbf{U}}_t$ so as to form M patches of $(k+1)$ points per patch, and $\mathbf{C}_t \in \mathbb{R}^{(k+1)M \times 3}$ contains the coordinates of patch centers for each point.

Specifically, as each patch is formed around a patch center, we first select M points from $\hat{\mathbf{U}}_t$ as the patch centers, denoted as $\{\mathbf{c}_{t,1}, \mathbf{c}_{t,2}, \dots, \mathbf{c}_{t,M}\} \in \mathbb{R}^{M \times 3} \subset \hat{\mathbf{U}}_t$. In order to keep the patches distributed as uniformly as possible, we first choose a random point in $\hat{\mathbf{U}}_t$ as $\mathbf{c}_{t,1}$, and add a point which holds the farthest distance to the previous patch centers as the next patch center, until there are M points in the set of patch centers. We then search the k -nearest neighbors of each patch center in terms of Euclidean distance, which leads to M patches in $\hat{\mathbf{U}}_t$.

B. Spatio-Temporal Similar Patch Search

Given each constructed patch in $\hat{\mathbf{U}}_t$, we search for its similar patches locally in $\hat{\mathbf{U}}_t$, and its corresponding patch in $\hat{\mathbf{U}}_{t-1}$ so as to exploit the spatio-temporal correlation. A metric is thus necessary to measure the similarity between patches, which remains challenging due to irregularity of patches. Taking two patches $\hat{\mathbf{p}}_{t,l}$ and $\hat{\mathbf{p}}_{t,m}$ in frame $\hat{\mathbf{U}}_t$ for instance, we discuss the similar patch search as follows. The temporally corresponding patches are searched in the same way.

1) *Similarity Metric*: We deploy a simplified approach of [13] to measure the similarity between two patches $\hat{\mathbf{p}}_{t,l}$ and $\hat{\mathbf{p}}_{t,m}$. The key idea is to compare the distance from each point in the two patches to the tangent plane at one patch center, which captures the similarity in geometric curvature of patches.

Firstly, we structure the tangent planes of two patches. As a point cloud essentially characterizes the continuous surface of 3D objects, we calculate the surface normals \mathbf{n}_l and \mathbf{n}_m for patch $\hat{\mathbf{p}}_{t,l}$ and patch $\hat{\mathbf{p}}_{t,m}$ respectively for structural description. Then we acquire the tangent planes of the two patches at the patch center $\mathbf{c}_{t,l}$ and $\mathbf{c}_{t,m}$ respectively.

Secondly, we measure patch similarity by the distance of each point in the two patches to the corresponding tangent plane. Specifically, we first project each point in patch $\hat{\mathbf{p}}_{t,l}$ and patch $\hat{\mathbf{p}}_{t,m}$ to the tangent plane of patch $\hat{\mathbf{p}}_{t,l}$. For the i -th point \mathbf{v}_l^i in patch $\hat{\mathbf{p}}_{t,l}$, we search a point \mathbf{v}_m^i in $\hat{\mathbf{p}}_{t,m}$, whose projection on the tangent plane is closest to that of \mathbf{v}_l^i . Denote by $d_l(\mathbf{v}_l^i)$ and $d_l(\mathbf{v}_m^i)$ the distance of the two points to their projections on the tangent plane of patch $\hat{\mathbf{p}}_{t,l}$, $|d_l(\mathbf{v}_l^i) - d_l(\mathbf{v}_m^i)|$ is regarded as the difference of the two patches in point \mathbf{v}_l^i and \mathbf{v}_m^i . Then we acquire the average difference between the two patches at all the $(k+1)$ points:

$$D_{l,m} = \sqrt{\frac{1}{k+1} \sum_{i=1}^{k+1} [d_l(\mathbf{v}_l^i) - d_l(\mathbf{v}_m^i)]^2}. \quad (17)$$

Similarly, projecting each point in patch $\hat{\mathbf{p}}_{t,l}$ and patch $\hat{\mathbf{p}}_{t,m}$ to the tangent plane of patch $\hat{\mathbf{p}}_{t,m}$, we acquire an average difference $D_{m,l}$. The final mean difference between the two patches is

$$\tilde{D}_{l,m} = \sqrt{\frac{1}{2}(D_{l,m}^2 + D_{m,l}^2)}. \quad (18)$$

2) *Local Patch Search*: Given a target patch in the t -th frame $\hat{\mathbf{p}}_{t,l}$, $l \in [1, M]$, we seek its r most similar patches within the current frame $\hat{\mathbf{U}}_t$ based on the similarity measure

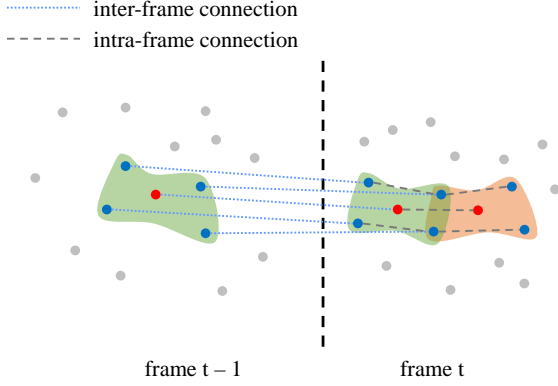


Fig. 3: Illustration of the spatio-temporal graph construction, including the inter-frame graph connection and intra-frame graph connection. In general, patches are overlapped within one frame, thus a point in one patch might be connected to its neighbor in the other patch in the overlapped region.

in (18), *i.e.*, $\{\hat{\mathbf{p}}_{t,m}\}_{m=1}^r$. As to the temporally corresponding patch in the previous frame $\tilde{\mathbf{U}}_{t-1}$, we only search the most similar one to $\hat{\mathbf{p}}_{t,l}$ as the corresponding patch $\tilde{\mathbf{p}}_{t-1,l}$.

Further, in order to reduce the computation complexity of global search, we set a *local* window in the t -th frame for fast similar patch search, which contains patches centering at the h -nearest neighbors of the target patch center in terms of Euclidean distance. Then we evaluate the similarity between the target patch and these h -nearest patches instead of all the patches in the t -th frame, which significantly improves the search efficiency.

Similarly, in the search of a temporally corresponding patch, we set a local window in the $(t-1)$ -th frame $\tilde{\mathbf{U}}_{t-1}$, which includes reference patches centering at the h -nearest neighbors of the collocated target patch center in terms of Euclidean distance. The reference patch with the largest similarity to the target patch is chosen as the temporally corresponding patch $\tilde{\mathbf{p}}_{t-1,l}$.

C. Proposed Spatio-Temporal Graph Connectivity

Having searched intra-frame similar patches and inter-frame corresponding patches, we build a spatio-temporal graph over the patches. The construction of intra-frame edge connectivities and inter-frame edge connectivities is based on patch similarity, as demonstrated in Fig. 3.

1) *Intra-frame graph connectivities*: Given a target patch $\hat{\mathbf{p}}_{t,l}$ in the t -th frame $\hat{\mathbf{U}}_t$, we construct a graph between $\hat{\mathbf{p}}_{t,l}$ and each of its similar patches $\hat{\mathbf{p}}_{t,m}$. Specifically, we connect each point in $\hat{\mathbf{p}}_{t,l}$ with its nearest neighbor in $\hat{\mathbf{p}}_{t,m}$, where the distance is in terms of their projections onto the tangent plane with orientation orthogonal to the surface normal of $\hat{\mathbf{p}}_{t,l}$ at the patch center of $\hat{\mathbf{p}}_{t,l}$. Similarly, each point in $\hat{\mathbf{p}}_{t,m}$ is connected with the nearest point in $\hat{\mathbf{p}}_{t,l}$ in terms of their projections onto the tangent plane orthogonal to the surface normal of $\hat{\mathbf{p}}_{t,m}$ at the patch center of $\hat{\mathbf{p}}_{t,m}$. Note that, we do not connect points within each patch explicitly, though an edge may exist between two points in a patch if they are also nearest neighbors in two different patches due to patch overlaps, as shown in Fig. 3.

2) *Inter-frame graph connectivities*: In order to leverage the inter-frame correlation and keep the temporal consistency, we connect corresponding patches between $\hat{\mathbf{U}}_t$ and $\tilde{\mathbf{U}}_{t-1}$. Similarly to the intra-graph construction, we connect each point in patch $\hat{\mathbf{p}}_{t,l}$ with its nearest point in patch $\tilde{\mathbf{p}}_{t-1,l}$, where the distance is in terms of their projections onto the tangent plane orthogonal to the surface normal of patch $\hat{\mathbf{p}}_{t,l}$ at the patch center of $\hat{\mathbf{p}}_{t,l}$. As such, we construct spatio-temporal graph connectivities as demonstrated in Fig. 3.

D. Formulation of Dynamic Point Cloud Denoising

We formulate dynamic point cloud denoising as an optimization problem for each underlying point cloud frame \mathbf{U}_t and distance metrics $\{\mathbf{R}_s, \mathbf{R}_t\}$, taking into account both inter-frame consistency and intra-frame smoothness.

Specifically, we seek the optimal \mathbf{U}_t , \mathbf{R}_s and \mathbf{R}_t to minimize an objective function including: 1) a data fidelity term, which enforces \mathbf{U}_t to be close to the observed noisy point cloud frame $\hat{\mathbf{U}}_t$; 2) a temporal consistency term, which promotes the consistency between each patch $\mathbf{P}_{t,i} \in \mathbb{R}^{(k+1) \times 3}$ in \mathbf{U}_t and its correspondence $\tilde{\mathbf{P}}_{t-1,i}$ in the reconstructed previous frame $\tilde{\mathbf{U}}_{t-1}$; 3) a spatial smoothness term, which enforces smoothness of each patch in \mathbf{U}_t with respect to the underlying graph encoded in the Laplacian $\mathbf{L}_t(\mathbf{R}_s) \in \mathbb{R}^{(k+1)M \times (k+1)M}$. The problem formulation is mathematically written as

$$\begin{aligned} \min_{\mathbf{U}_t, \mathbf{R}_s, \mathbf{R}_t} & \|\mathbf{U}_t - \hat{\mathbf{U}}_t\|_2^2 + \lambda_1 \sum_{i=1}^M \|\sqrt{\mathbf{w}_i(\mathbf{R}_t)^\top} (\mathbf{P}_{t,i} - \tilde{\mathbf{P}}_{t-1,i})\|_2^2 \\ & + \lambda_2 \text{tr}(\mathbf{P}_t^\top \mathbf{L}_t(\mathbf{R}_s) \mathbf{P}_t), \\ \text{s.t.} & \mathbf{P}_t = \mathbf{S}_t \mathbf{U}_t - \mathbf{C}_t, \end{aligned} \quad (19)$$

where each element of $\mathbf{w}_i(\mathbf{R}_t) \in \mathbb{R}^{k+1}$ is the edge weight between a pair of temporally corresponding points for the i -th patch. λ_1 and λ_2 are weighting parameters for the trade-off among the data fidelity term, the temporal consistency term and the spatial smoothness term. For the simplicity of notation, we define a diagonal matrix $\mathbf{W}_{t,t-1} \in \mathbb{R}^{(k+1)M \times (k+1)M}$ to describe the temporal weights \mathbf{w}_i between corresponding patches:

$$\mathbf{W}_{t,t-1} = \text{diag} \left[\underbrace{\sqrt{w_{1,1}} \cdots \sqrt{w_{1,k+1}}}_{k+1} \cdots \underbrace{\sqrt{w_{M,1}} \cdots \sqrt{w_{M,k+1}}}_{k+1} \right]. \quad (20)$$

Substituting $\mathbf{W}_{t,t-1}$ and the constraint into the objective of (19), we have

$$\begin{aligned} & \|\mathbf{U}_t - \hat{\mathbf{U}}_t\|_2^2 \\ \min_{\mathbf{U}_t, \mathbf{R}_s, \mathbf{R}_t} & + \lambda_1 \|\mathbf{W}_{t,t-1}(\mathbf{R}_t)(\mathbf{S}_t \mathbf{U}_t - \mathbf{C}_t) - \mathbf{W}_{t,t-1}(\mathbf{R}_t) \tilde{\mathbf{P}}_{t-1}\|_2^2 \\ & + \lambda_2 \text{tr}((\mathbf{S}_t \mathbf{U}_t - \mathbf{C}_t)^\top \mathbf{L}_t(\mathbf{R}_s)(\mathbf{S}_t \mathbf{U}_t - \mathbf{C}_t)). \end{aligned} \quad (21)$$

(21) is nontrivial to solve with three optimization variables. Next, we develop an alternating minimization approach to solve (21).

E. Proposed Algorithm for Dynamic Point Cloud Denoising

We propose to address (21) by alternately optimizing the underlying point cloud frame \mathbf{U}_t and the distance metrics \mathbf{R}_s and \mathbf{R}_t . The iterations terminate when the difference in the objective between two consecutive iterations stops decreasing.

In particular, we first perform denoising on the first frame of a point cloud sequence exploiting available intra-correlations (*i.e.*, $\lambda_1 = 0$). Then for the subsequent frame, we take advantage of the *reconstructed* previous frame as better reference than the noisy version.

1) *Optimizing the distance metrics \mathbf{R}_s and \mathbf{R}_t* : We first initialize \mathbf{U}_t with the noisy observation $\hat{\mathbf{U}}_t$, and optimize \mathbf{R}_s and \mathbf{R}_t via spatio-temporal graph learning described in Section IV. Spatial and temporal edge weights are then computed from the learned \mathbf{R}_s and \mathbf{R}_t respectively via (8), which lead to \mathbf{L}_t and $\mathbf{W}_{t,t-1}$ in (21).

In particular, we consider two types of features on point clouds: Cartesian coordinates and angles between surface normals. We adopt surface normals to promote smoothness of the underlying surface. Specifically, we employ a function of the angle $\theta_{i,j}$ between two normals \mathbf{n}_i and \mathbf{n}_j as the feature difference in surface normals at points i and j as follows

$$d_{\theta_{i,j}} = 1 - |\cos \theta_{i,j}| = 1 - \left| \frac{\mathbf{n}_i \cdot \mathbf{n}_j}{\|\mathbf{n}_i\| \|\mathbf{n}_j\|} \right|. \quad (22)$$

Along with the feature difference in three-dimensional coordinates, we form a four-dimensional feature difference vector $\mathbf{f}_i - \mathbf{f}_j = [x_i - x_j, y_i - y_j, z_i - z_j, d_{\theta_{i,j}}]^\top$, where x_i, y_i, z_i denote the coordinate of point i and x_j, y_j, z_j the coordinate of point j . Based on the constructed spatio-temporal graph connectives discussed in Section V-C, we then employ the feature difference at each pair of spatially connected points to learn the spatial metric \mathbf{R}_s , and the feature difference at each pair of temporally connected points to learn the temporal metric \mathbf{R}_t as described in Section IV.

2) *Optimizing the point cloud \mathbf{U}_t* : With both \mathbf{L}_t and $\mathbf{W}_{t,t-1}$ fixed from the learned \mathbf{R}_s and \mathbf{R}_t , we take the derivative of (21) with respect to \mathbf{U}_t and set the derivative to 0. This leads to the closed-form solution of \mathbf{U}_t :

$$\begin{aligned} & (\mathbf{I} + \lambda_1 \mathbf{S}_t^\top \mathbf{W}_{t,t-1}^\top \mathbf{W}_{t,t-1} \mathbf{S}_t + \lambda_2 \mathbf{S}_t^\top \mathbf{L}_t \mathbf{S}_t) \mathbf{U}_t \\ &= \hat{\mathbf{U}}_t + \lambda_1 \mathbf{S}_t^\top \mathbf{W}_{t,t-1}^\top \mathbf{W}_{t,t-1} (\mathbf{C}_t + \tilde{\mathbf{P}}_{t-1}) + \lambda_2 \mathbf{S}_t^\top \mathbf{L}_t \mathbf{C}_t, \end{aligned} \quad (23)$$

where $\mathbf{I} \in \mathbb{R}^{n \times n}$ is an identity matrix. (23) is a system of linear equations and thus can be solved efficiently. Then we employ the acquired solution of \mathbf{U}_t to update \mathbf{R}_s and \mathbf{R}_t in the subsequent iteration.

A flowchart of the dynamic point cloud denoising algorithm is demonstrated in Fig. 2, and an algorithmic summary is presented in Algorithm 1.

Algorithm 1: 3D Dynamic Point Cloud Denoising

Input: A noisy dynamic point cloud sequence $\hat{\mathcal{P}} = \{\hat{\mathbf{U}}_1, \hat{\mathbf{U}}_2, \dots, \hat{\mathbf{U}}_m\}$

Output: Denoised dynamic point cloud sequence $\tilde{\mathcal{P}} = \{\tilde{\mathbf{U}}_1, \tilde{\mathbf{U}}_2, \dots, \tilde{\mathbf{U}}_m\}$

```

1 for  $\hat{\mathbf{U}}_t$  in  $\hat{\mathcal{P}}$  do
2   Initialize  $\tilde{\mathbf{U}}_t$  with  $\hat{\mathbf{U}}_t$ 
3   Select  $M$  points (set  $\mathbf{C}_t$ ) as patch centers;
4   for  $\mathbf{c}_l$  in  $\mathbf{C}_t$  do
5     Find  $k$ -nearest neighbors of  $\mathbf{c}_l$ ;
6     Build patch  $\hat{\mathbf{p}}_{t,l}$ ;
7     Add  $\hat{\mathbf{p}}_{t,l}$  to the patch set  $\hat{\mathbf{P}}_t$ ;
8   end
9   repeat
10    for  $\hat{\mathbf{p}}_{t,l}$  in  $\hat{\mathbf{P}}_t$  do
11      Search the  $r$  most similar patches of  $\hat{\mathbf{p}}_{t,l}$  in  $\hat{\mathbf{U}}_t$  in terms of the metric in (18);
12      for  $\hat{\mathbf{p}}_{t,j}$  in  $\hat{\mathbf{p}}_{t,l}$ 's similar patches do
13        | Connect nearest points in  $\hat{\mathbf{p}}_{t,l}$  and  $\hat{\mathbf{p}}_{t,j}$ ;
14      end
15      Search the corresponding patch  $\tilde{\mathbf{p}}_{t-1,l}$  of  $\hat{\mathbf{p}}_{t,l}$  in  $\tilde{\mathbf{U}}_{t-1}$  via (18);
16      Connect corresponding points in  $\hat{\mathbf{p}}_{t,l}$  and  $\tilde{\mathbf{p}}_{t-1,l}$ ;
17    end
18    Learn the spatial metric  $\mathbf{R}_s$  from spatially connected point pairs via (9), and compute the intra-frame graph Laplacian  $\mathbf{L}_t$  via (8);
19    Learn the temporal metric  $\mathbf{R}_t$  from temporally connected point pairs via (9), and compute the weight matrix  $\mathbf{W}_{t,t-1}$  between corresponding patches via (8);
20    Solve (23) to update  $\tilde{\mathbf{U}}_t$ ;
21  until convergence;
22   $\tilde{\mathbf{U}}_t$  serves as the input for denoising the next frame.
23 end

```

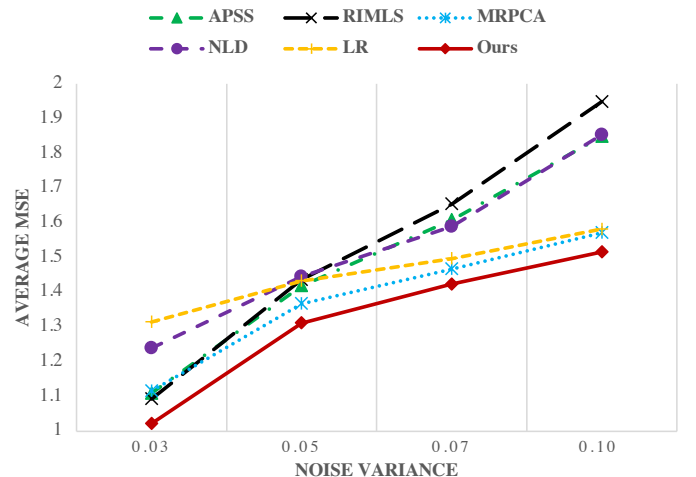


Fig. 4: Comparison between different methods in terms of the average MSE under various noise levels.

TABLE I: MSE comparison for different models with Gaussian noise.

Model	Noisy	APSS	RIMLS	MRPCA	NLD	LR	Baseline1	Baseline2	Ours
$\sigma = 0.03$									
Soldier	1.4984	1.4125	1.3572	1.3488	1.6148	1.7850	1.2979	1.3227	1.2976
Longdress	1.4746	1.3985	1.3360	1.3247	1.5900	1.7751	1.2722	1.2996	1.2704
Loot	1.4715	1.3571	1.3279	1.3101	1.5751	1.6997	1.2434	1.2618	1.2433
Redandblack	1.4589	1.3892	1.3499	1.3221	1.6040	1.7701	1.2663	1.3024	1.2663
Andrew	0.8874	0.8839	0.8894	0.9655	0.9582	0.9745	0.8294	0.8302	0.8283
David	0.9421	0.9131	0.9247	0.9487	0.9581	0.9558	0.8516	0.8527	0.8513
Phil	0.8732	0.8686	0.8752	0.9553	0.9589	0.9706	0.8171	0.8163	0.8154
Ricardo	0.9113	0.8994	0.9042	0.9449	0.9567	0.9587	0.8251	0.8275	0.8250
Sarah	0.8808	0.8677	0.8731	0.9257	0.9394	0.9425	0.8045	0.8079	0.8045
Average	1.1554	1.1100	1.0931	1.1162	1.2395	1.3147	1.0231	1.0357	1.0225
$\sigma = 0.05$									
Soldier	2.1453	1.8047	1.8105	1.8116	1.9465	1.9767	1.7654	1.7907	1.7606
Longdress	2.1260	1.8007	1.7955	1.7922	1.9306	1.9601	1.7428	1.7839	1.7382
Loot	2.1286	1.7668	1.7883	1.7703	1.9317	1.8949	1.7121	1.7320	1.7018
Redandblack	2.1110	1.7915	1.8061	1.7939	1.9389	1.9650	1.7423	1.7871	1.7351
Andrew	1.1516	1.1154	1.1359	1.0433	1.0532	1.0331	0.9852	0.9859	0.9841
David	1.2014	1.1562	1.1817	1.0217	1.0598	1.0123	0.9703	0.9713	0.9701
Phil	1.1478	1.1027	1.1253	1.0426	1.0541	1.0351	0.9864	0.9857	0.9844
Ricardo	1.1720	1.1276	1.1541	1.0220	1.0513	1.0160	0.9881	0.9602	0.9596
Sarah	1.1533	1.1020	1.1281	1.0107	1.0376	1.0035	0.9705	0.9701	0.9686
Average	1.5930	1.4186	1.4362	1.3676	1.4449	1.4330	1.3181	1.3297	1.3114
$\sigma = 0.07$									
Soldier	2.5417	1.9675	2.0450	1.9999	2.156	2.0758	1.9551	1.9753	1.9356
Longdress	2.5139	1.9630	2.0297	1.9754	2.1324	2.0561	1.9409	1.9667	1.9275
Loot	2.5205	1.9359	2.0271	1.9487	2.1276	1.9950	1.8951	1.8990	1.8848
Redandblack	2.5035	1.9726	2.0537	1.9849	2.1421	2.0639	1.9807	1.9807	1.9284
Andrew	1.3241	1.3113	1.3295	1.0739	1.1482	1.0681	1.0408	1.0390	1.0378
David	1.3903	1.3821	1.3988	1.0516	1.1690	1.0519	1.0263	1.0262	1.0256
Phil	1.3202	1.2984	1.3192	1.0774	1.1423	1.0739	1.0456	1.0445	1.0431
Ricardo	1.3524	1.3388	1.3580	1.0528	1.1542	1.0542	1.0116	1.0121	1.0103
Sarah	1.3292	1.3080	1.3291	1.0413	1.1293	1.0390	1.0211	1.0230	1.0208
Average	1.8662	1.6086	1.6545	1.4673	1.5890	1.4975	1.4352	1.4407	1.4238
$\sigma = 0.10$									
Soldier	3.0127	2.1404	2.3901	2.1874	2.4887	2.1813	2.1097	2.1049	2.0610
Longdress	2.9761	2.1236	2.3748	2.1360	2.4683	2.1506	2.0650	2.0941	2.0475
Loot	2.9853	2.1118	2.3338	2.1037	2.4664	2.0935	2.0080	2.0224	1.9941
Redandblack	2.9622	2.1433	2.3266	2.1563	2.4636	2.1640	2.0814	2.1213	2.0586
Andrew	1.5615	1.5916	1.5911	1.1203	1.3473	1.1326	1.1149	1.1098	1.1087
David	1.6621	1.7045	1.6959	1.1166	1.4193	1.1400	1.0772	1.0710	1.0682
Phil	1.5581	1.5850	1.5849	1.1296	1.3288	1.1408	1.1333	1.1257	1.1246
Ricardo	1.6068	1.6392	1.6390	1.1098	1.3698	1.1333	1.0811	1.0800	1.0800
Sarah	1.5740	1.6000	1.6031	1.0829	1.3284	1.1044	1.1078	1.1041	1.1035
Average	2.2110	1.8488	1.9488	1.5714	1.8534	1.5823	1.5309	1.5370	1.5162

VI. EXPERIMENTAL RESULTS

A. Experimental Setup

We evaluate our algorithm by testing on two benchmarks, including four MPEG sequences (*Longdress*, *Loot*, *Redandblack* and *Soldier*) from [34] and five MSR sequences (*Andrew*, *David*, *Phil*, *Ricardo* and *Sarah*) from [3]. We randomly choose six consecutive frames as the sample data: frame 601-606 in *Soldier*, frame 1201-1206 in *Loot*, frame 1201-1206 in *Longdress*, frame 1501-1506 in *Redandblack*, frame 61-66 in *Andrew*, frame 61-66 in *David*, frame 61-66 in *Phil*, frame 61-66 in *Ricardo* and frame 61-66 in *Sarah*. We perform down-sampling with the sampling rate of 0.05 prior to denoising since the number of points in each frame is about 1 million. Because point clouds in the datasets are clean in general, we add white Gaussian noise with a range of variance $\sigma = \{0.03, 0.05, 0.07, 0.1\}$.

Due to the lack of previous dynamic point cloud denoising approaches, we compare our algorithm with five competitive static point cloud denoising methods: APSS [5], RIMLS [6],

MRPCA [11], NLD [28], and LR [29]. We perform each static denoising method frame by frame independently on dynamic point clouds. We employ two evaluation metrics: Mean Squared Error (MSE) and Signal-to-Noise Ratio (SNR) as in [16].

The parameter settings are as follows. We assign the upper-bound C of the trace of \mathbf{R} in (9) as 10. The step size t of the PG algorithm in (15) is assigned as 0.0001. In (21), the weighting parameter of the temporal consistency term λ_1 is set to 0.003, while that of the spatial smoothness term λ_2 is set to 0.1. Besides, given the first frame in each dataset, we set $\lambda_1 = 0$ as there is no previous frame for reference. We divide each point cloud into $M = 0.2n$ patches, where n is the number of points in the point cloud. Each patch is connected with $r = 8$ most similar patches spatially.

B. Experimental Results

1) *Objective results:* We list the denoising results of comparison methods measured in MSE and SNR respectively

TABLE II: SNR comparison for different models with Gaussian noise.

Model	Noisy	APSS	RIMLS	MRPCA	NLD	LR	Baseline1	Baseline2	Ours
$\sigma = 0.03$									
Soldier	60.5080	61.0895	61.4889	58.8487	59.7501	58.7476	61.9348	61.7464	61.9364
Longdress	60.2722	61.0876	61.3056	58.9989	59.7318	58.6296	61.9514	61.7425	61.9765
Loot	60.4739	61.0155	61.4740	58.7771	59.5969	58.8364	61.9617	61.8158	61.9625
Redandblack	61.9718	62.4682	62.7552	60.0590	61.0298	60.0439	63.3921	63.1114	63.3925
Andrew	60.6087	60.6634	60.6013	59.7802	59.8401	59.6678	61.3751	61.3089	61.3751
David	61.8615	62.1288	62.0025	61.7464	61.6924	61.7124	62.9836	62.9715	62.9789
Phil	61.0185	61.0715	60.9958	60.1201	60.0825	59.9568	61.8027	61.7344	61.8022
Ricardo	61.8591	61.3581	61.3049	60.8649	61.3659	61.3384	62.8508	62.8199	62.8502
Sarah	61.5861	61.7562	61.6941	61.1092	60.9420	60.9047	62.4779	62.4360	62.4775
Average	61.1289	61.4043	61.5136	60.0338	60.4480	59.9820	62.3033	62.1874	62.3057
$\sigma = 0.05$									
Soldier	56.9009	58.6395	58.6073	57.2701	57.8826	57.7279	58.8591	58.7170	58.9019
Longdress	56.6003	58.4490	58.3288	57.2296	57.7906	57.6380	58.8139	58.5815	58.8409
Loot	56.8114	58.4876	58.5077	57.1579	57.6307	57.7497	58.7638	58.6480	58.8241
Redandblack	58.2667	59.9247	59.8431	58.4732	59.1330	58.9989	60.2008	59.9473	60.2422
Andrew	58.0028	58.3371	58.1550	59.0052	58.8956	59.0832	59.6320	59.5540	59.6384
David	59.4297	59.7683	59.5502	61.0052	60.6839	61.1377	61.6321	61.6308	61.6428
Phil	58.2839	58.6850	58.4821	59.2455	59.1356	59.3136	59.8755	59.7854	59.8823
Ricardo	59.3394	59.0967	58.8644	60.0804	60.4224	60.7580	61.3232	61.2826	61.3291
Sarah	58.8916	59.3658	59.1317	60.2308	59.9485	60.2776	60.7052	60.6659	60.7102
Average	58.0585	58.9726	58.8300	58.8553	59.0581	59.1872	59.9784	59.8681	60.0013
$\sigma = 0.07$									
Soldier	55.2291	57.7755	57.3897	56.7700	56.8600	57.2386	57.8381	57.7361	57.9548
Longdress	54.9225	57.5355	57.0761	56.7004	56.7966	57.1599	57.8408	57.6060	57.8578
Loot	55.1564	57.6245	57.2908	56.6518	56.5903	57.2345	57.8537	57.7271	57.8798
Redandblack	56.5859	58.9614	58.5588	57.9666	58.1366	58.5079	59.1883	58.9168	59.2297
Andrew	56.6060	56.7192	56.5814	58.7164	58.0317	58.7508	59.0601	59.0068	59.0885
David	57.9697	57.9839	57.8638	60.7169	59.7034	60.7551	61.1491	61.1794	61.1718
Phil	56.8851	57.0514	56.8925	58.9173	58.3323	58.9459	59.2335	59.1642	59.2661
Ricardo	57.9082	57.3803	57.2380	59.7839	59.4909	60.3900	60.8283	60.8178	60.8535
Sarah	57.4719	57.6519	57.4919	59.9323	59.1013	59.9301	60.1309	60.1041	60.1467
Average	56.5261	57.6315	57.3759	58.4617	58.1159	58.7681	59.2359	59.1398	59.2721
$\sigma = 0.10$									
Soldier	53.5216	56.9332	55.8305	56.4273	55.7253	56.7428	57.0740	57.0984	57.3077
Longdress	53.1795	56.6672	55.6671	56.3759	55.6710	56.7106	57.1137	56.9744	57.1986
Loot	53.4494	56.8385	55.7228	56.3343	55.4772	56.7527	57.1631	57.0917	57.2321
Redandblack	54.8903	58.1316	57.0985	57.6910	57.0420	58.0349	58.4176	58.2291	58.5282
Andrew	54.9534	54.7820	54.7851	58.2932	56.4331	58.1644	58.1091	58.1559	58.3518
David	56.1841	55.8875	55.9380	60.1174	57.7633	59.9503	60.4625	60.5199	60.5469
Phil	55.2281	55.0572	55.0578	58.4442	56.8196	58.3415	58.1000	58.1810	58.3842
Ricardo	56.1872	55.3559	55.3571	59.2565	57.7833	59.6694	60.1116	60.0769	60.2444
Sarah	55.7812	55.6373	55.6179	59.5410	57.4776	59.3387	59.1646	59.2422	59.3179
Average	54.8194	56.1434	55.6750	58.0534	56.6880	58.1895	58.4129	58.3966	58.5680

in Tab. I and Tab. II, and mark the lowest MSE/SNR in bold. Our method outperforms all the five static point cloud denoising approaches on the nine datasets at all the noise levels on average. Specifically, we achieve reduction of the MSE by 11.90% on average over APSS, 14.00% on average over RIMLS, 4.50% on average over MRPCA, 13.92% on average over NLD, and 9.50% on average over LR. The results are also visualized in Fig. 4 for easy comparison. This validates the effectiveness of our method.

2) *Ablation studies*: To evaluate the two main contributions of our method—temporal consistency and spatio-temporal graph learning, we conduct two baselines for comparison. In *Baseline1*, we remove the temporal consistency term in (21) to evaluate the importance of temporal references, *i.e.*, $\lambda_1 = 0$. Only similar patches in the same frame are employed as the reference for denoising in this case, where the underlying spatial graph is acquired from the proposed learning of spatial distance metric. For the evaluation of spatio-temporal graph learning, in *Baseline2* we set edge weights

as a Gaussian function with manually assigned parameters $\mathbf{M} = \mathbf{I}$ instead of the proposed graph learning, *i.e.*, $a_{i,j} = \exp\{-(\mathbf{f}_i - \mathbf{f}_j)^\top(\mathbf{f}_i - \mathbf{f}_j)\}$.

As presented in Tab. I and Tab. II, we outperform both *Baseline1* and *Baseline2* constantly. Specifically, we achieve reduction of MSE over *Baseline1* by 0.63% on average at all noise levels, and over *Baseline2* by 1.30% on average. In particular, we achieve larger gain over dynamic point clouds with *slower motion* due to the stronger temporal correlation. For instance, the average MSE reduction over the comparatively static *Redandblack* is 1.16%, while that over *Sarah* is 0.17% with much more dynamic motion in the tested frames. Further, the MSE reduction over *Baseline1* is 0.06%, 0.51%, 0.79%, 0.96% respectively with increasing noise levels. This indicates that the temporal correlation plays a more important role at high noise levels.

3) *Subjective results*: As illustrated in Fig. 5 and Fig. 6, the proposed method also improves the visual results significantly, especially in local details and temporal consistency. In order to

demonstrate the temporal consistency, we choose 5 consecutive frames that exhibit apparent movement in *Andrew* from the MSR benchmark and *Longdress* from the MPEG benchmark, both under the noise variance $\sigma = 0.05$. We show the visual comparison with MRPCA and LR because they are the nearest two competitors to our method in objective performance, as presented in Fig. 4.

We see that our results preserve the local structure and keep the temporal consistency better. For instance, in the *Andrew* model, while the results of LR and MRPCA still exhibit noisy contours even with outliers along the shoulder, our results are much smoother and cleaner. Also, note that, the ground truth of *Andrew* is a little bit noisy due to the inherent limitation of the acquisition equipment—RGBD cameras, while our method is able to attenuate the sensor noise well. In *Longdress*, while the nose of the model is over-smoothing and even distorted in shape in the results of LR and MRPCA, our method preserves the structure of the nose much better. Further, our results are much more consistent in the temporal domain, which validates the effectiveness of the spatio-temporal graph learning.

VII. CONCLUSION

We propose 3D dynamic point cloud denoising based on spatio-temporal graph learning, exploiting both the intra-frame self-similarity and inter-frame consistency. Assuming the availability of a relevant feature vector per node on a point cloud sequence, we pose spatio-temporal graph learning as the problem of Mahalanobis distance metric learning, where we minimize the Graph Laplacian Regularizer and decompose the symmetric and positive-definite metric matrix for ease of optimization via proximal gradient. Then we formulate dynamic point cloud denoising as the joint optimization of the desired point cloud and underlying spatio-temporal graph, which is regularized by both intra-frame smoothness among searched similar patches and inter-frame consistency between corresponding patches. Experimental results show that our method significantly outperforms independent denoising of each frame from state-of-the-art static point cloud denoising approaches.

REFERENCES

- [1] R. B. Rusu and S. Cousins, “3d is here: Point cloud library (pcl),” *IEEE International Conference on Robotics and Automation*, pp. 1–4, 2011.
- [2] C. Tulvan, R. Mekuria, Z. Li, and S. Laserre, “Use cases for point cloud compression,” in *ISO/IEC JTC1/SC29/WG11 (MPEG) output document N16331*, June 2016.
- [3] C. Loop, Q. Cai, S. O. Escolano, and P. A. Chou, “Microsoft voxelized upper bodies—a voxelized point cloud dataset,” in *ISO/IEC JTC1/SC29 Joint WG11/WG1 (MPEG/JPEG) input document m38673/M72012*, 2016.
- [4] M. Alexa, J. Behr, D. Cohen-Or, S. Fleishman, D. Levin, and C. T. Silva, “Computing and rendering point set surfaces,” *IEEE Transactions on Visualization and Computer Graphics*, vol. 9, no. 1, pp. 0–15, 2003.
- [5] G. Guennebaud and M. Gross, “Algebraic point set surfaces,” in *ACM SIGGRAPH*, 2007, p. 23.
- [6] C. Oztireli, G. Guennebaud, and M. Gross, “Feature preserving point set surfaces based on non-linear kernel regression,” vol. 28, pp. 493–501, 2009.
- [7] H. Huang, S. Wu, M. Gong, D. Cohen-Or, and H. Zhang, “Edge-aware point set resampling,” *ACM Transactions on Graphics (TOG)*, vol. 32, no. 1, pp. 1–12, 2013.
- [8] H. Hui, L. Dan, Z. Hao, U. Ascher, and D. Cohen-Or, “Consolidation of unorganized point clouds for surface reconstruction,” in *Acm Siggraph Asia*, 2009.
- [9] Y. Lipman, D. Cohen-Or, D. Levin, and H. Tal-Ezer, “Parameterization-free projection for geometry reconstruction,” *Acm Transactions on Graphics*, vol. 26, no. 3, p. 22, 2007.
- [10] H. Avron, A. Sharf, C. Greif, and D. Cohen-Or, “11-sparse reconstruction of sharp point set surfaces,” *ACM Transactions on Graphics (TOG)*, vol. 29, p. 135, 10 2010.
- [11] E. Mattei and A. Castrodad, “Point cloud denoising via moving rpca,” *Computer Graphics Forum*, vol. 36, 11 2017.
- [12] C. Dinesh, G. Cheung, I. V. Bajic, and Y. Cheng, “Fast 3d point cloud denoising via bipartite graph approximation & total variation,” 2018.
- [13] Z. Jin, G. Cheung, M. Ng, J. Pang, and Y. Cheng, “3d point cloud denoising using graph laplacian regularization of a low dimensional manifold model,” (accepted to) *IEEE Transactions on Image Processing*, December 2019.
- [14] C. Dinesh, G. Cheung, and I. V. Bajic, “3d point cloud denoising via bipartite graph approximation and reweighted graph laplacian,” *arXiv preprint arXiv:1812.07711*, 2018.
- [15] Z. Jin, G. Cheung, M. Ng, J. Pang, and Y. Cheng, “3D point cloud denoising using graph laplacian regularization of a low dimensional manifold model,” *accepted to IEEE Transactions on Image Processing*, December 2019.
- [16] C. Duan, S. Chen, and J. Kovacevic, “Weighted multi-projection: 3d point cloud denoising with estimated tangent planes,” *arXiv preprint arXiv:1807.00253*, 2018.
- [17] W. Hu, X. Gao, G. Cheung, and Z. Guo, “Feature graph learning for 3d point cloud denoising,” *accepted to IEEE Transactions on Signal Processing*, February 2019.
- [18] P. C. Mahalanobis, “On the generalized distance in statistics,” *Proceedings of the National Institute of Sciences of India*, vol. 2, no. 1, pp. 49–55, 1936.
- [19] J. Pang and G. Cheung, “Graph laplacian regularization for image denoising: Analysis in the continuous domain,” *IEEE Transactions on Image Processing (TIP)*, vol. 26, no. 4, pp. 1770–1785, 2017.
- [20] F. R. Chung, “Spectral graph theory,” in *Conference Board of the Mathematical Sciences*, no. 92. American Mathematical Society, 1997.
- [21] N. Parikh and S. Boyd, “Proximal algorithms,” *Foundations and Trends in Optimization*, vol. 1, no. 3, pp. 123–231, 2013.
- [22] Y. Schoenenberger, J. Paratte, and P. Vandergheynst, “Graph-based denoising for time-varying point clouds,” in *3DTV-Conference: The True Vision-Capture*, 2015.
- [23] Y. Sun, S. Schaefer, and W. Wang, *Denoising point sets via L 0 minimization*, 2015.
- [24] A. Buades, B. Coll, and J.-M. Morel, “A non-local algorithm for image denoising,” in *IEEE Conference on Computer Vision and Pattern Recognition (CVPR)*, vol. 2, 2005, pp. 60–65.
- [25] K. Dabov, A. Foi, V. Katkovnik, and K. Egiazarian, “Image denoising by sparse 3-d transform-domain collaborative filtering,” *IEEE Transactions on Image Processing (TIP)*, vol. 16, no. 8, pp. 2080–2095, Aug 2007.
- [26] J. Digne, “Similarity based filtering of point clouds,” in *IEEE Conference on Computer Vision and Pattern Recognition Workshops (CVPRW)*, 2012, pp. 73–79.
- [27] G. Rosman, A. Dubrovina, and R. Kimmel, “Patch-collaborative spectral point-cloud denoising,” in *Computer Graphics Forum*, vol. 32, no. 8. Wiley Online Library, 2013, pp. 1–12.
- [28] J. E. Deschaud and F. Goulette, “Point cloud non local denoising using local surface descriptor similarity,” *International Archives of Photogrammetry and Remote Sensing (IAPRS)*, vol. 38, pp. 109–114, 2010.
- [29] K. Sarkar, F. Bernard, K. Varanasi, C. Theobalt, and D. Stricker, “Structured low-rank matrix factorization for point-cloud denoising,” in *International Conference on 3D Vision (3DV)*, 2018, pp. 444–453.
- [30] G. Shen, W. S. Kim, S. K. Narang, A. Ortega, and H. C. Wey, “Edge-adaptive transforms for efficient depth map coding,” in *IEEE Picture Coding Symposium (PCS)*, December 2010, pp. 566–569.
- [31] W. Hu, G. Cheung, A. Ortega, and O. C. Au, “Multiresolution graph fourier transform for compression of piecewise smooth images,” *IEEE Transactions on Image Processing (TIP)*, vol. 24, pp. 419–433, January 2015.
- [32] D. Spielman, “Lecture 2 of spectral graph theory and its applications,” September 2004.
- [33] C. Tomasi and R. Manduchi, “Bilateral filtering for gray and color images,” in *International Conference on Computer Vision (ICCV)*, vol. 98, no. 1, 1998, p. 2.
- [34] T. Ebner, I. Feldmann, O. Schreer, P. Kauff, and T. Unger, “Hhi point cloud dataset of a boxing trainer,” in *ISO/IEC JTC1/SC29/WG11 (MPEG2018) input document M42921*, July 2018.



Fig. 5: Comparison results with Gaussian noise $\sigma = 0.05$ for *Andrew*: (a) The ground truth; (b) The noisy point cloud; (c) The denoised result by LR; (d) The denoised result by MRPCA; (e) The denoised result by our algorithm. Colors are not shown in the magnified regions for clear demonstration of geometry denoising.



Fig. 6: Comparison results with Gaussian noise $\sigma = 0.05$ for *Longdress*: (a) The ground truth; (b) The noisy point cloud; (c) The denoised result by LR; (d) The denoised result by MRPCA; (e) The denoised result by our algorithm. Colors are not shown in the magnified regions for clear demonstration of geometry denoising.